Optimized Pulse Patterns for Synchronous Machines with Non-Sinusoidal Back-EMF

Eleftherios Kontodinas*, Petros Karamanakos*, Andreas Kraemer†, and Sebastian Wendel†
*Tampere University, Faculty of Information Technology and Communication Sciences
33101 Tampere, Finland
†ZF Friedrichshafen AG
97424 Schweinfurt, Germany
Email: eleftherios.kontodinas@tuni.fi, p.karamanakos@ieee.org, andreas.kraemer@zf.com, sebastian.wendel@zf.com

ACKNOWLEDGMENTS

This work was supported in part by ZF Friedrichshafen AG and in part by the Academy of Finland.

***Index Terms*—Electric vehicle (EV), pulse width modulation (PWM), optimal efficiency drive, optimization, permanent magnet motor, voltage source inverter (VSI)**

***Abstract*—Permanent magnet synchronous machines (PMSMs) used in automotive applications typically have a small number of stator slots. This distorts the air-gap flux distribution, thus resulting in a non-sinusoidal back-electromotive force (back-EMF), which in turn deteriorates the drive performance and decreases its efficiency. To address this, this paper proposes optimized pulse patterns (OPPs) that account for the back-EMF harmonics. In doing so, the computed OPPs can significantly improve the drive performance in terms of current and torque distortions. The presented numerical results verify the effectiveness of the proposed modulation method.**

I. INTRODUCTION

Interior permanent magnet synchronous machines (IPMSMs) are widely used in automotive applications due to their high power density, high efficiency, and low maintenance requirements. Ideally, the IPMSMs would be supplied by sinusoidal currents. In practice, however, there are always current harmonics that induce extra losses. The primary source of harmonic distortions is the switching nature of the converter, while the secondary is the motor construction imperfections. To produce high-quality current waveforms, and thus improve the efficiency of the drive train, advanced control and/or modulation methods that account for the load characteristics and the spatial harmonics can be utilized.

The distribution of the stator winding and the slot effect result in spatial harmonics on the flux linkage. These harmonics give, in turn, rise to back-electromotive force (EMF) harmonics on the windings, increasing the stator current harmonic content. Therefore, additional losses and heating are generated, resulting in lower motor efficiency [1]. Moreover, back-EMF harmonics can cause torque ripples that have an adverse effect on the output torque, as they can lead to vibrations and noise in the motor, thus eventually compromising the quality and reliability of the overall system [2].

To address the additional losses caused by a non-sinusoidal back-EMF, several control strategies have been developed over the last few years. For example, with the help of either a losses approximation model or an online back-EMF harmonics identification, [1] and [3] augmented conventional current control methods with appropriate harmonic voltage injection to counteract the back-EMF harmonics. Moreover, alternative solutions have been proposed, such as methods that employ neural-network-based current harmonics suppression mechanisms [4].

The aforementioned methods can be used in conjunction with asynchronous pulse width modulation (PWM) techniques and thus can be reasonably effective when the fundamental-to-switching frequency ratio is big. In automotive applications, however, motors are used at higher speeds, meaning that the electrical fundamental frequency can be high, and thus close to the switching frequency. At such low pulse numbers, these applications require more sophisticated modulation methods to achieve high-quality current, such as optimized pulse

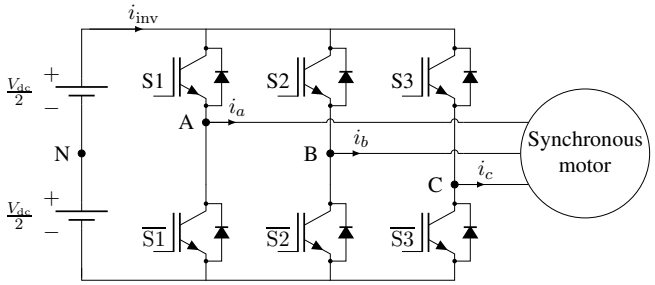

Fig. 1: Electrical drive system consisting of a two-level inverter and a synchronous motor.

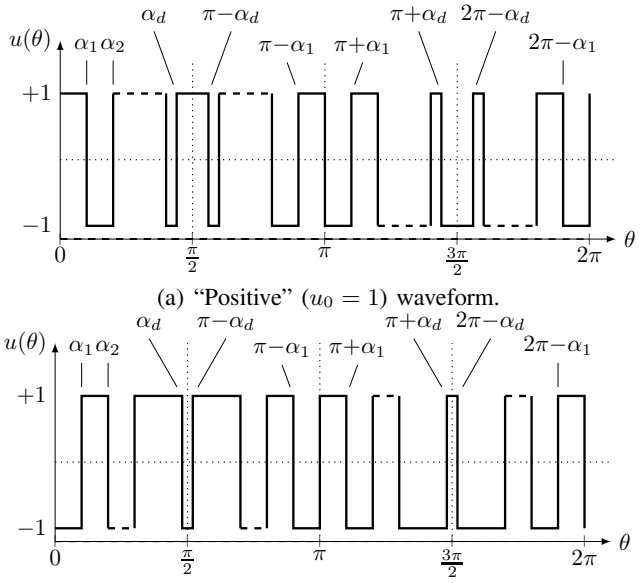

(a) "Positive" ($u_0 = 1$) waveform.

(b) "Negative" ($u_0 = -1$) waveform.

Fig. 2: Two-level switched waveform with QaHWS.

patterns (OPPs) [5], [6]. As shown in [7], conventional OPPs applied to low-voltage automotive-grade IPMSMs result in minimum harmonic distortions, thus increasing the total system efficiency.

Despite the fact that aforementioned OPPs can significantly outperform conventional PWM methods, they are calculated assuming that the motor is a purely inductive load. Therefore, when the OPPs calculation accounts for the load properties further performance improvements can be achieved. This was verified in [8], [9], where the magnetic anisotropy properties of the machine were considered in the optimization procedure. In doing so, the objective function of the OPP optimization problem depends not only on the modulation index—as is the case with the conventional OPPs—but also on the load angle, and the saliency ratio.

Motivated by the benefits that the tailored, load-friendly OPPs computed in [8], [9] can bring, this paper goes one step further by proposing OPPs that also account for the back-EMF harmonics of the machine. To this aim, the synchronous machine model used for the formulation of the OPP problem is refined such that the effect of the back-EMF harmonics is also considered [10]. In doing so, the proposed OPPs can mitigate the adverse effects of the spatial harmonics and, consequently, improve the quality of the stator and dc-link current as well as of the torque, as demonstrated with the presented numerical results acquired with an IPMSM drive system used in automotive applications.

II. System Modeling

A. Output Voltage of Synchronous Modulation

Considering the system of Fig. 1, the electric drive that serves as a case study consists of a two-level voltage-source converter connected to a synchronous motor with a non-sinusoidal back-EMF. Assuming synchronous modulation, the output voltage of the converter, i.e., the voltage applied to the machine, is a sequence of $q = f_{\text{sw}}/f_1 \in \mathbb{N}^+$ pulses per fundamental period, where f_{sw} is the switching frequency and f_1 the fundamental frequency, respectively. This three-phase voltage is given by

$$\boldsymbol{v}_{s,abc} = \frac{V_{\text{dc}}}{2}\boldsymbol{u}_{abc}\,, \tag{1}$$

where V_{dc} is the dc-link voltage, and $\boldsymbol{u}_{abc} = [u_a \;\; u_b \;\; u_c]^\top \in \{-1, 1\}^3$ is the three-phase switch position.

Assuming a three-phase balanced system, it suffices to focus on the switched waveform of phase a, i.e., $u \equiv u_a$, for the analysis of the three-phase output converter voltage that follows. Moreover, it is common practice with synchronous modulation to impose quarter- and half- wave symmetry (QaHWS) on the switched waveform $u(\theta)$, i.e.,

$$u(\theta) = u(\pi - \theta)\,,$$

holds for quarter-wave symmetry, and

$$u(\theta) = -u(\pi + \theta)\,,$$

for half-wave symmetry. As a result, the switched waveform has $d = (q-1)/2, d \in \mathbb{N}^+$ switching angles $\alpha_i \in [0, \pi/2], i \in \{1, \ldots, d\}$, that need to be computed in an optimization process such that the modulation goals will be met.

Based on the above symmetry properties, and since $u(\theta)$ is a periodic signal, it can be represented by the following Fourier series

$$u(\theta) = a_0 + \sum_{n=1}^{\infty} \left(a_n \cos(n\theta) + b_n \sin(n\theta)\right), \tag{2}$$

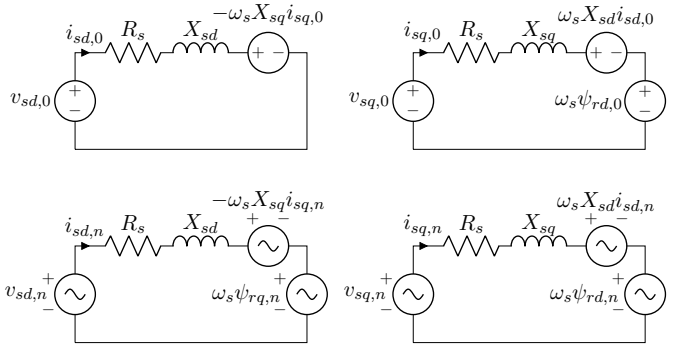

Fig. 3: Equivalent circuit diagrams in rotating reference frame for a synchronous motor with non-sinusoidal back-EMF.

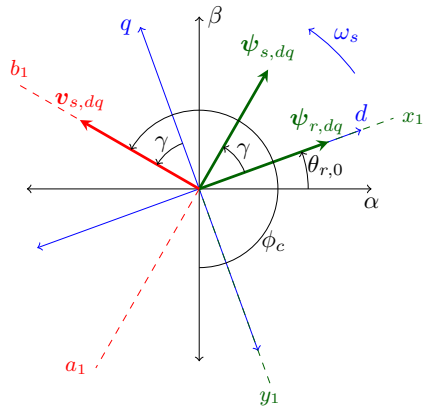

Fig. 4: Vector diagram of a synchronous motor

where n is the harmonic order. Due to the QaHWS, the Fourier coefficients α_0 and α_n are zero, while the b_n coefficients are

$$b_n = \begin{cases} u_0 \frac{4}{n\pi} \left(1 + 2\sum_{i=1}^{d} (-1)^i \cos(n\alpha_i)\right), & n = 1, 3, 5, \dots \\ 0\,. & n = 2, 4, 6, \dots \end{cases} \tag{3}$$

Finally, it is worth noting that in the case of the two-level converter, two different types of waveforms are introduced depending on the position of the switch at the beginning of the period, as shown in Fig. 2. More specifically, the first switch position can be either positive, i.e., $u_0 = 1$ (see Fig. 2(a)), or negative, i.e., $u_0 = -1$ as shown in Fig. 2(b).

B. Stator Voltage in a Rotating Reference Frame

For a better description of the synchronous machine, the equivalent circuit in the orthogonal, rotating (dq) frame is employed (see Fig. 3). In this model, the harmonics of the rotor flux and the anisotropy of the machine can be considered. Moreover, the vector diagram in Fig. 4 facilitates the analysis of the electrical analysis. In the said vector diagram, the d-axis of the rotating frame is aligned with the rotor flux vector $\boldsymbol{\psi}_{r,dq}$, which rotates counterclockwise with the synchronous angular speed ω_s. The angle $\theta_{r,0}$ is the initial phase between the α-axis of the stationary ($\alpha\beta$) frame and the rotor flux vector. The red dashed lines indicate the position of the a_1 and b_1 Fourier coefficients of the stator voltage with a ϕ_c initial displacement. Since the imposed QaHWS on the switched waveform results in $a_1 = 0$ and $b_1 = m$. the stator voltage vector is aligned with the axis of the b_1 Fourier coefficient. Furthermore, as the considered IPMSM is predominantly an inductive load (with a non-sinusoidal back-EMF), it is assumed that $R_s \approx 0$. Due to this assumption, the voltage vector $\boldsymbol{v}_{s,dq}$ becomes perpendicular to the stator flux vector $\boldsymbol{\psi}_{s,dq}$, and thus the angle between the $\boldsymbol{v}_{s,dq}$ and the q-axis is equal to the load angle γ.

For the derivation of the analysis that follows, it is assumed that the rotor flux vector is initially aligned with the α-axis, i.e., $\theta_{r,0} = 0$, implying that $\phi_c = \gamma + \pi$. Moreover, by considering the rotor angle $\theta_r = \omega_s t$—which indicates the position of the frame—it follows that the stator voltage angle in the rotating frame is $\theta_{\boldsymbol{v}_{s,dq}} = \theta_r + \phi_c$. Therefore, the stator voltage in the abc-frame is

$$\boldsymbol{v}_{s,abc}(\theta_r + \phi_c) = \begin{bmatrix} v_{sa}(\theta_r + \phi_c) \\ v_{sb}(\theta_r + \phi_c - \frac{2\pi}{3}) \\ v_{sc}(\theta_r + \phi_c - \frac{4\pi}{3}) \end{bmatrix}. \tag{4}$$

With (4), and the help of the Park transformation, the stator voltage in the dq-frame is given by

$$\boldsymbol{v}_{s,dq} = \boldsymbol{R}(\theta_r)\boldsymbol{K}\boldsymbol{v}_{s,abc}(\theta_r + \phi_c)\,, \tag{5}$$

where

$$\boldsymbol{R}(\theta_r) = \begin{bmatrix} \cos(\theta_r) & \sin(\theta_r) \\ -\sin(\theta_r) & \cos(\theta_r) \end{bmatrix}, \quad \boldsymbol{K} = \frac{2}{3}\begin{bmatrix} 1 & -\frac{1}{2} & -\frac{1}{2} \\ 0 & \frac{\sqrt{3}}{2} & -\frac{\sqrt{3}}{2} \end{bmatrix}.$$

C. Rotor Flux Harmonics in a Rotating Reference Frame

Consider the three-phase rotor flux $\boldsymbol{\psi}_{r,abc} = [\psi_{ra}\ \psi_{rb}\ \psi_{rc}]^\top$, with $\psi_{rb}(\theta_r) = \psi_{ra}(\theta_r - \frac{2\pi}{3})$ and $\psi_{rc}(\theta_r) = \psi_{ra}(\theta_r - \frac{4\pi}{3})$. Assuming that the dc-component is zero, then the a-phase rotor flux has the following Fourier representation

$$\psi_{ra}(\theta_r) = \sum_{n=1}^{\infty} x_n \cos(n\theta_r) + y_n \sin(n\theta_r)\,. \tag{6}$$

In Fig. 4, the green dashed lines indicate the positions of x_1 and y_1 Fourier coefficients of the rotor flux. The calculation of the rotor flux Fourier coefficients in

synchronous excited motors can be done from the open-circuit stator voltage measurement. The voltage equation at the stationary reference frame is

$$\boldsymbol{v}_{s,abc} = R_s \boldsymbol{i}_{s,abc} + \frac{\mathrm{d}\boldsymbol{\psi}_{s,abc}}{\mathrm{d}t}\,. \tag{7}$$

As an open circuit is assumed, it follows that $\boldsymbol{i}_{s,abc} = \mathbf{0}$ and $\boldsymbol{\psi}_{s,abc} = \boldsymbol{\psi}_{r,abc}$. Therefore, the a-phase rotor flux can be written with the help of (7) as

$$\psi_{ra} = \int v_{sa}\mathrm{d}t. \tag{8}$$

Considering that the measured a-phase stator voltage Fourier representation is

$$v_{sa} = \sum_{n=1}^{\infty} \Big(\zeta_n \cos(n\theta_r) + \xi_n \sin(n\theta_r)\Big), \tag{9}$$

where ζ_n and ξ_n correspond to the v_{sa} Fourier coefficients, the a-phase rotor flux can be calculated from (8) as

$$\begin{aligned}\psi_{ra} &= \int \left(\sum_{n=1}^{\infty} \Big(\zeta_n \cos(n\theta_r) + \xi_n \sin(n\theta_r)\Big)\right)\mathrm{d}t \\ \psi_{ra} &= \sum_{n=1}^{\infty} \Big(-\frac{\xi_n}{n}\cos(n\theta_r) + \frac{\zeta_n}{n}\sin(n\theta_r)\Big)\,.\end{aligned} \tag{10}$$

Hence, by recalling (6), it follows that the flux Fourier coefficients can be written as a function of the Fourier coefficients of the measured back-EMF as

$$x_n = -\frac{\xi_n}{n}\,, \quad \text{and} \quad y_n = \frac{\zeta_n}{n}\,.$$

Finally, considering that the rotor flux vector $\boldsymbol{\psi}_{r,dq}$ is aligned with the d-axis and its angle is equal to the angle of the rotating frame, it can obtained from the abc-frame flux through

$$\boldsymbol{\psi}_{r,dq} = \boldsymbol{R}(\theta_r)\boldsymbol{K}\boldsymbol{\psi}_{r,abc}(\theta_r)\,.$$

D. Stator Current in a Rotating Reference Frame

The continuous-time domain voltage equations of a synchronous machine in the dq-frame are

$$v_{sd} = R_s i_{sd} + \frac{\mathrm{d}\psi_{sd}}{\mathrm{d}t} - \omega_s \psi_{sq}\,, \tag{11a}$$

$$v_{sq} = R_s i_{sq} + \frac{\mathrm{d}\psi_{sq}}{\mathrm{d}t} + \omega_s \psi_{sd}\,, \tag{11b}$$

where the stator flux is

$$\psi_{sd} = X_{sd} i_{sd} + \psi_{rd}\,, \tag{12a}$$

$$\psi_{sq} = X_{sq} i_{sq} + \psi_{rq}\,, \tag{12b}$$

where X_{sd} and X_{sq} are the stator reactances on the d- and q-axis, respectively, while the cross coupling terms are neglected. By transforming (11) into the frequency domain, and with the help of (12), the stator voltage is given by

$$\begin{bmatrix} v_{sd} \\ v_{sq} \end{bmatrix} = \begin{bmatrix} R_s + sX_{sd} & -\omega_s X_{sq} \\ \omega_s X_{sd} & R_s + sX_{sq} \end{bmatrix} \begin{bmatrix} i_{sd} \\ i_{sq} \end{bmatrix} + \begin{bmatrix} s & -\omega_s \\ \omega_s & s \end{bmatrix} \begin{bmatrix} \psi_{rd} \\ \psi_{rq} \end{bmatrix} \tag{13}$$

where s = $\jmath n\omega_s$. Hence, the stator current in dq-frame is given by

$$\begin{bmatrix} i_{sd} \\ i_{sq} \end{bmatrix} = \begin{bmatrix} R_s + sX_{sd} & -\omega_s X_{sq} \\ \omega_s X_{sd} & R_s + sX_{sq} \end{bmatrix}^{-1} \left(\begin{bmatrix} v_{sd} \\ v_{sq} \end{bmatrix} - \begin{bmatrix} s & -\omega_s \\ \omega_s & s \end{bmatrix} \begin{bmatrix} \psi_{rd} \\ \psi_{rq} \end{bmatrix} \right). \tag{14}$$

By adopting phasors to represent complex variables, the expression for the harmonic ($n > 0$) current frequency response can derived based on (14). By assuming $R_s = 0$, this yields

$$\begin{aligned} \begin{bmatrix} i_{sd,n} \\ i_{sq,n} \end{bmatrix} &= \begin{bmatrix} M_{dd,n}\angle\theta_{dd,n} & M_{dq,n}\angle\theta_{dq,n} \\ M_{qd,n}\angle\theta_{qd,n} & M_{qq,n}\angle\theta_{qq,n} \end{bmatrix} \begin{bmatrix} v_{sd,n} \\ v_{sq,n} \end{bmatrix} \\ &\quad + \begin{bmatrix} Q_{dd,n}\angle\varphi_{dd,n} & Q_{dq,n}\angle\varphi_{dq,n} \\ Q_{qd,n}\angle\varphi_{qd,n} & Q_{qq,n}\angle\varphi_{qq,n} \end{bmatrix} \begin{bmatrix} \psi_{rd,n} \\ \psi_{rq,n} \end{bmatrix}, \end{aligned} \tag{15}$$

where the magnitudes $M_{xx,n}$ and angles $\theta_{xx,n}$ are

$$\begin{aligned} M_{dd,n} &= \frac{\chi}{\omega_s X_{sq}} \frac{n}{(n^2-1)}\,, \quad \theta_{dd,n} = -\frac{\pi}{2}\,, \\ M_{dq,n} &= \frac{\chi}{\omega_s X_{sq}} \frac{1}{(n^2-1)}\,, \quad \theta_{dq,n} = \pi\,, \\ M_{qd,n} &= \frac{1}{\omega_s X_{sq}} \frac{1}{(n^2-1)}\,, \quad \theta_{qd,n} = 0\,, \\ M_{qq,n} &= \frac{1}{\omega_s X_{sq}} \frac{n}{(n^2-1)}\,, \quad \theta_{qq,n} = -\frac{\pi}{2}\,, \end{aligned}$$

with $\chi = X_{sq}/X_{sd}$ being the saliency ratio. Similarly, the magnitudes $Q_{xx,n}$ and angles $\varphi_{xx,n}$ are

$$\begin{aligned} Q_{dd,n} &= \frac{\chi}{X_{sq}}\,, \quad \varphi_{dd,n} = \pi\,, \\ Q_{dq,n} &= 0\,, \quad \varphi_{dq,n} = 0\,, \\ Q_{qd,n} &= 0\,, \quad \varphi_{qd,n} = 0\,, \\ Q_{qq,n} &= \frac{1}{X_{sq}}\,, \quad \varphi_{qq,n} = \pi\,. \end{aligned}$$

E. Stator Current Total Demand Distortion

The harmonic content of the stator current can result in iron and copper losses, and thus thermal losses, in the machine. The total demand distortion (TDD) is employed as an index of the current quality, which is given by

$$I_{s,\mathrm{TDD}} = \frac{1}{\sqrt{2} I_{s,\mathrm{nom}}} \sqrt{\sum_{n\neq 1} (\hat{i}_{sa,n})^2}\,, \tag{16}$$

where the phase current (phase a above) can be obtained from the inverse Clarke transformation, i.e.,

$$\boldsymbol{i}_{s,abc} = \boldsymbol{K}^{-1}\boldsymbol{R}^{-1}(\theta_r)\boldsymbol{i}_{s,dq}\,.$$

Note that in (16), $I_{s,\mathrm{nom}}$ stands for the rms value of the nominal current. By employing the above analysis, the stator current TDD is derived in (17), where

$$\begin{aligned}
\mathcal{H}_1(\boldsymbol{\alpha},\chi,\gamma) &= +\,b_{n+1}\frac{\chi-1}{n+1}\sin(2\gamma)\,,\\
\mathcal{H}_2(\boldsymbol{\alpha},\chi,\gamma) &= -\,b_{n-1}\frac{\chi+1}{n-1} - b_{n+1}\frac{\chi-1}{n+1}\cos(2\gamma)\,,\\
\mathcal{H}_3(\boldsymbol{\alpha},\chi,\gamma) &= -\,b_{n-1}\frac{\chi-1}{n-1}\sin(2\gamma)\,,\\
\mathcal{H}_4(\boldsymbol{\alpha},\chi,\gamma) &= -\,b_{n+1}\frac{\chi+1}{n+1} - b_{n-1}\frac{\chi-1}{n-1}\cos(2\gamma)\,,
\end{aligned}$$

are the factors that depend on the saliency ratio χ, and the load angle γ. Moreover, they depend on the switching angles $\boldsymbol{\alpha} = [\alpha_1\ \alpha_2\ \ldots\ \alpha_d]^\top$ as they are a function of the b_n Fourier coefficients of the switching function $u(\theta)$.

III. Optimized Pulse Patterns

A. Objective Function

The OPPs are computed in an offline optimization procedure that typically aims to minimize the stator current distortion. To do so, an objective function that captures the harmonic content of the stator current as a function of the optimization variable, i.e., the switching angles $\boldsymbol{\alpha}$, is required. Studying expression (17), it can be observed that it is the product of a scaling factor and a function J. The latter is a function of the switching angles $\boldsymbol{\alpha}$, saliency ratio χ, load angle γ, dc-link voltage V_{dc}, and the synchronous speed ω_s. Therefore, this function J serves as the objective function in the optimization problem, while the scaling factor is discarded as it does not affect the results of the optimization procedure.

TABLE I: Parameters of the IPMSM drive system

Parameter	Value	Parameter	Value
Nominal voltage V_N	926 V	Nominal frequency f_1	120 Hz
Nominal current I_N	138 A	Pole pairs	4
Nominal power P_N	190 kW	Dc-link voltage V_{dc}	800 V
Stator resistance R_s	0.046 Ω	Power factor	0.86
d-axis inductance L_{sd}	1.58 mH	PM flux linkage λ_{PM}	0.684 Wb
q-axis inductance L_{sq}	3.32 mH		

For OPPs to be applicable over the whole range of operation, they are typically computed for a discrete number of modulation indices m in the equidistantly gridded interval $[0, \pi/4]$. Since R_s is neglected, the $\frac{V_{\mathrm{dc}}}{2\omega_s}$ term in the objective function J from (17) can be written as a function of the modulation index, as follows

$$\begin{aligned}
\|\boldsymbol{v}_{s,dq}\| &= \|\boldsymbol{\psi}_{s,dq}\|\omega_s \Leftrightarrow\\
m\frac{V_{\mathrm{dc}}}{2} &= \|\boldsymbol{\psi}_{s,dq}\|\omega_s \Leftrightarrow\\
\frac{V_{\mathrm{dc}}}{2\omega_s} &= \frac{\|\boldsymbol{\psi}_{s,dq}\|}{m}\,,
\end{aligned} \tag{18}$$

where $\|\boldsymbol{\psi}_{s,dq}\|$ is the stator flux magnitude. Considering that for synchronous motors with anisotropy the current reference $\boldsymbol{i}^*_{s,dq}$ at each load angle γ is typically obtained from the maximum torque per ampere (MTPA) curve, the stator flux magnitude $\|\boldsymbol{\psi}_{s,dq}\|$ changes with the load angle γ, i.e.,

$$\|\boldsymbol{\psi}_{s,dq}(\gamma)\| = \left\| \begin{bmatrix} X_{sd} & 0 \\ 0 & X_{sq} \end{bmatrix} \boldsymbol{i}^*_{s,dq}(\gamma) + \begin{bmatrix} \psi_{rd,0} \\ \psi_{rq,0} \end{bmatrix} \right\|. \tag{19}$$

Therefore, with (18) and (19), the chosen objective function from (17) takes its final form and becomes a function of the switching angle $\boldsymbol{\alpha}$, the saliency ratio χ, the load angle γ, and the modulation index m.

$$\begin{aligned}
I_{s,\mathrm{TDD}} = \overbrace{\frac{1}{2\sqrt{2}I_{s,\mathrm{nom}}X_{sq}}}^{\text{scaling factor}} \overbrace{\Bigg(}^{\text{objective function } J(\boldsymbol{\alpha},\chi,\gamma,V_{\mathrm{dc}},\omega_s)}
&\sum_{n=6k}^{\infty}\Bigg(-\frac{V_{\mathrm{dc}}}{2\omega_s}\Big(\mathcal{H}_1(\boldsymbol{\alpha},\chi,\gamma)\cos((n-1)\gamma) - \mathcal{H}_2(\boldsymbol{\alpha},\chi,\gamma)\sin((n-1)\gamma)\Big) - \Big((\chi-1)y_{n+1} + (\chi+1)y_{n-1}\Big)\Bigg)^2\\
+&\sum_{n=6k}^{\infty}\Bigg(-\frac{V_{\mathrm{dc}}}{2\omega_s}\Big(\mathcal{H}_1(\boldsymbol{\alpha},\chi,\gamma)\sin((n-1)\gamma) + \mathcal{H}_2(\boldsymbol{\alpha},\chi,\gamma)\cos((n-1)\gamma)\Big) - \Big((\chi-1)x_{n+1} + (\chi+1)x_{n-1}\Big)\Bigg)^2\\
+&\sum_{n=6k}^{\infty}\Bigg(-\frac{V_{\mathrm{dc}}}{2\omega_s}\Big(\mathcal{H}_3(\boldsymbol{\alpha},\chi,\gamma)\cos((n+1)\gamma) - \mathcal{H}_4(\boldsymbol{\alpha},\chi,\gamma)\sin((n+1)\gamma)\Big) - \Big((\chi+1)y_{n+1} + (\chi-1)y_{n-1}\Big)\Bigg)^2\\
+&\sum_{n=6k}^{\infty}\Bigg(-\frac{V_{\mathrm{dc}}}{2\omega_s}\Big(\mathcal{H}_3(\boldsymbol{\alpha},\chi,\gamma)\sin((n+1)\gamma) + \mathcal{H}_4(\boldsymbol{\alpha},\chi,\gamma)\cos((n+1)\gamma)\Big) - \Big((\chi+1)x_{n+1} + (\chi-1)x_{n-1}\Big)\Bigg)^2\Bigg)^{\frac{1}{2}}
\end{aligned} \tag{17}$$

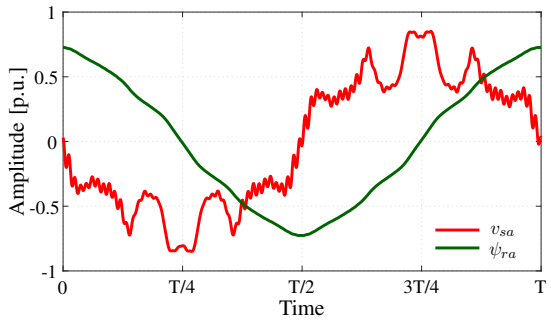

(a) Open-circuit measured back-EMF v_{sa} at nominal speed and calculated rotor flux ψ_{ra}

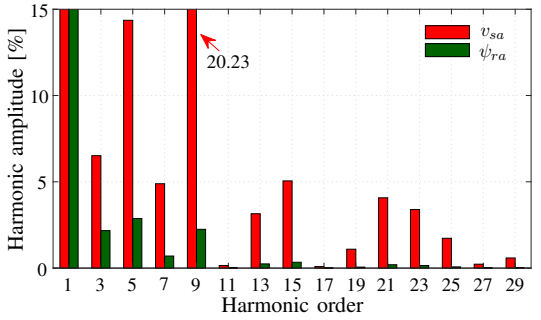

(b) Back-EMF and rotor flux harmonic spectra

Fig. 5: Non-sinusoidal back-EMF of the IPMSM.

B. Optimization Problem

To calculate the OPPs in question, the following optimization problem is formulated based on the aforementioned objective function

$$\underset{\boldsymbol{\alpha}\in[0,\frac{\pi}{2}]^d}{\text{minimize}} \quad J(\boldsymbol{\alpha},\chi,\gamma,m) \tag{20a}$$

$$\text{subject to} \quad u_0\frac{4}{\pi}\left(1+2\sum_{i=1}^{d}(-1)^i\cos(\alpha_i)\right)=m \tag{20b}$$

$$0\leq\alpha_1\leq\alpha_2\cdots\leq\alpha_d\leq\frac{\pi}{2}. \tag{20c}$$

Problem (20) aims to compute the optimal vector of switching angles vector d, and it is solved for each possible combination of the saliency ratio χ, load angle γ, and modulation index m. Note that in (20), the equality constraints (20b) ensure that the amplitude of the fundamental component is equal to the desired modulation index $m \in [0, 4/\pi]$, while the inequality constraints (20c) guarantee that the switching angles are within $[0, \pi/2]$ and in ascending order.

IV. Effects of the Back-EMF Harmonics on the Motor Performance

This section analyzes the effect of a non-sinusoidal back-EMF on the performance of an automotive-grade IPMSM. The drive parameters are described in Table I. From the open-circuit test at nominal speed, the measured phase-a voltage is shown in Fig. 5(a), which corresponds to the back-EMF. The rotor flux is calculated as described in Section II-C. The harmonic spectra of the back-EMF and the rotor flux linkage are shown in Fig. 5(b). Therein the amplitude of the harmonics is presented as a percentage of the fundamental component. As can be observed, the non-zero harmonics are of odd order. However, given that common-mode harmonics (i.e., triplen harmonics) do not drive harmonic current in a balanced three-phase system, only the differential-mode harmonics contribute to the current harmonics. Thus, the main harmonics that have an adverse effect on the current quality are the 5^{th} and the 7^{th} rotor flux harmonics.

For an automotive drive, the most relevant performance metrics are the stator current TDD ($I_{s,\text{TDD}}$), the electromagnetic torque TDD ($T_{e,\text{TDD}}$), and the dc-link current TDD ($I_{\text{inv,TDD}}$). To illustrate the effect of the back-EMF of Fig. 5(a) on those metrics, a direct comparison with the same motor with a sinusoidal back-EMF is performed. More specifically, the drive system is first simulated assuming a sinusoidal back-EMF and then assuming the back-EMF of Fig. 5(a) for torque in the range of $T_e \in [0, 1]$ per unit (p.u.) and over the whole range of achievable modulation indices, i.e., $m \in [0, 4/\pi]$. Conventional OPPs, i.e., OPPs that do not account for the anisotropy of the machine are applied in both drive systems. Finally, to provide more insight into the discussed comparisons, the relative TDD of each chosen metric is calculated as

$$\delta_{\text{TDD,rel,1}}=\frac{\delta_{\text{TDD}}\left(\begin{smallmatrix}\text{non-sinusoidal}\\ \text{back-EMF}\end{smallmatrix}\right)-\delta_{\text{TDD}}\left(\begin{smallmatrix}\text{sinusoidal}\\ \text{back-EMF}\end{smallmatrix}\right)}{\delta_{\text{TDD}}\left(\begin{smallmatrix}\text{sinusoidal}\\ \text{back-EMF}\end{smallmatrix}\right)}\cdot 100\% \tag{21}$$

where $\delta \in \{I_s, T_e, I_{\text{inv}}\}$, where the performance of conventional OPPs applied to a drive with a sinusoidal back-EMF is used for benchmarking purposes.

Given the above-mentioned framework, Fig. 6 presents the relative performance metrics for conventional OPPs with $d = 7$ and $d = 11$. As can be seen, the rotor flux harmonics can have a significant negative impact on the stator current and electromagnetic torque TDDs, resulting in performance degradation and efficiency reduction. The impact of these harmonics becomes more pronounced with an increasing modulation index as the influence of the back-EMF is greater at higher speeds. As for the dc-link current, this is less susceptible to back-EMF harmonics. Notwithstanding the foregoing, the harmonic content of I_{inv} is also

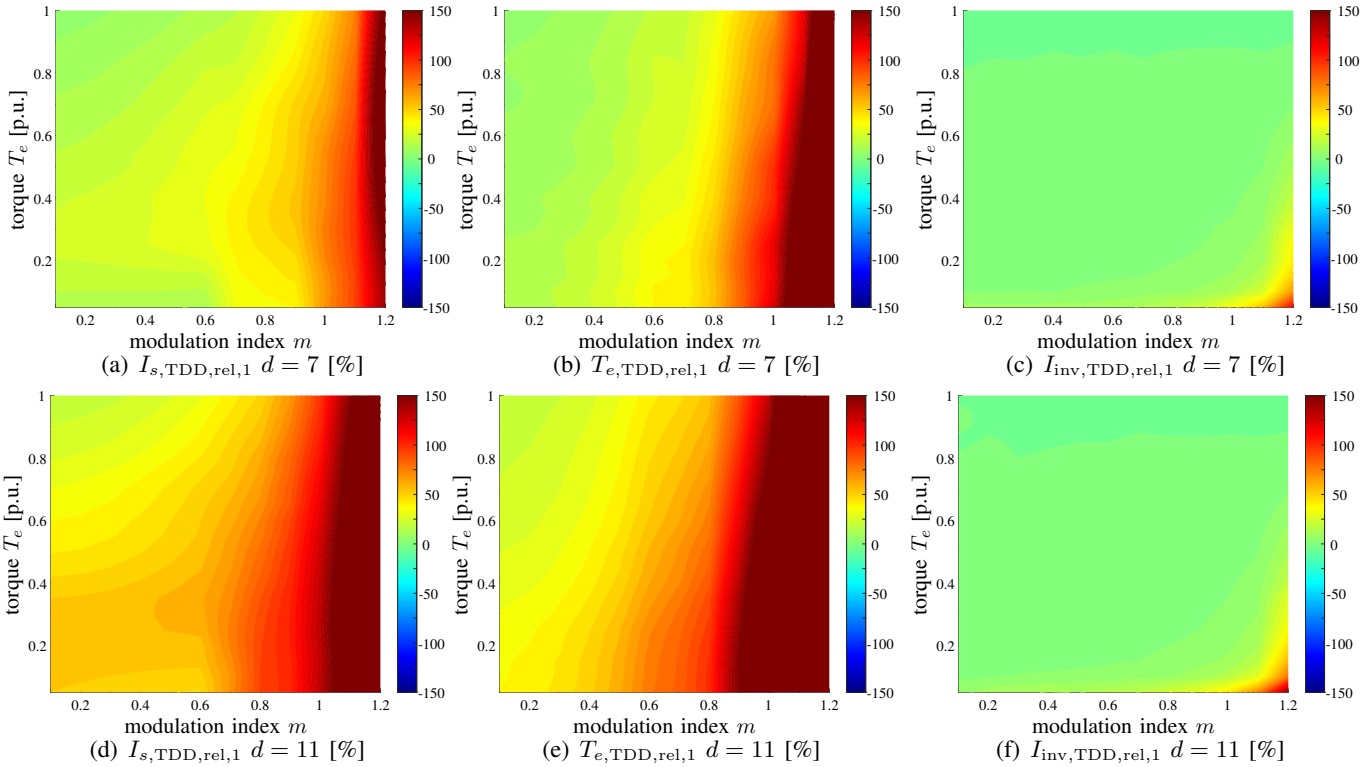

(a) $I_{s,\mathrm{TDD,rel,1}}$ $d=7$ [%] (b) $T_{e,\mathrm{TDD,rel,1}}$ $d=7$ [%] (c) $I_{\mathrm{inv,TDD,rel,1}}$ $d=7$ [%]

(d) $I_{s,\mathrm{TDD,rel,1}}$ $d=11$ [%] (e) $T_{e,\mathrm{TDD,rel,1}}$ $d=11$ [%] (f) $I_{\mathrm{inv,TDD,rel,1}}$ $d=11$ [%]

Fig. 6: Relative performance metrics of the motor with non-sinusoidal back-EMF with respect to the motor with sinusoidal back-EMF when isotropic QaHWS OPPs are applied.

increased in the high-speed/low-torque area.

V. OPPs Performance Evaluation

The optimization problem derived in Section III-B is solved for $d = 7$ and 11 and for the whole range of modulation indices, i.e., $m \in [0,\, 4/\pi]$. The saliency ratio of the IPMSM is $\chi = 2.1$, while load angles in the range $\gamma \in [1^o,\, 90^o]$ are considered. For this study, the IPMSM with the non-sinusoidal back-EMF of Fig. 5(a) is employed. The performance of the computed OPPs—hereafter referred to as back-EMF OPPs—is assessed in terms of $I_{s,\mathrm{TDD}}$, $T_{e,\mathrm{TDD}}$, and $I_{\mathrm{inv,TDD}}$. As previously, the relative TDD of each metric is employed to provide meaningful comparisons. To this end, conventional (isotropic) OPPs serve as the benchmark, and the relative performance metrics are calculated as

$$\delta_{\mathrm{TDD,rel,2}} = \frac{\delta_{\mathrm{TDD}}(\text{back-EMF OPPs}) - \delta_{\mathrm{TDD}}(\text{conv OPPs})}{\delta_{\mathrm{TDD}}(\text{conv OPPs})} \cdot 100\% \tag{22}$$

where $\delta \in \{I_s,\, T_e,\, I_{\mathrm{inv}}\}$.

From the results in Fig. 7, the performance benefits of the proposed back-EMF OPPs can be confirmed. Especially for the $I_{s,\mathrm{TDD}}$, it can be observed that back-EMF OPPs outperform the conventional OPPs over the whole operating range. The significant reduction in the low-torque/high-speed region can be highly beneficial for automotive applications. In this region, where an automotive drive system usually operates when cruising at higher speeds, the back-EMF OPPs results in up to a 40% and 48% reduction in current TDD for $d = 7$ and $d = 11$, respectively.

In terms of torque TDD, the proposed back-EMF OPPs can be beneficial for most operating points, but there are regions where $T_{e,\mathrm{TDD}}$ increases.

As the OPP optimization problem 20 aims to minimize the current harmonic distortions, while accounting for the back-emf harmonics and the anisotropy of the machine, it can only indirectly improve the torque harmonics. However, this cannot be achieved for all operating points; due to the anisotropic nature of the motor, i.e., the higher inductance on the q-axis, the current quality on the q-axis can be somewhat compromised in the overall aim to effectively mitigate the current harmonics. In doing so, the torque harmonics increase. Even though, as shown in [11], this issue can be addressed by appropriately formulating the OPP problem, this work does not account for the torque harmonics. Hence, the increase in the torque TDD is unavoidable, as can be seen in the range $T_e \in [0.2,\ 0.4]$, where it can reach up to 18% for both $d = 7$, and $d = 11$. However, for $T_e \in [0,\, 0.2] \cup [0.4,\, 0.9]$ the reduction in $T_{e,\mathrm{TDD}}$ is up

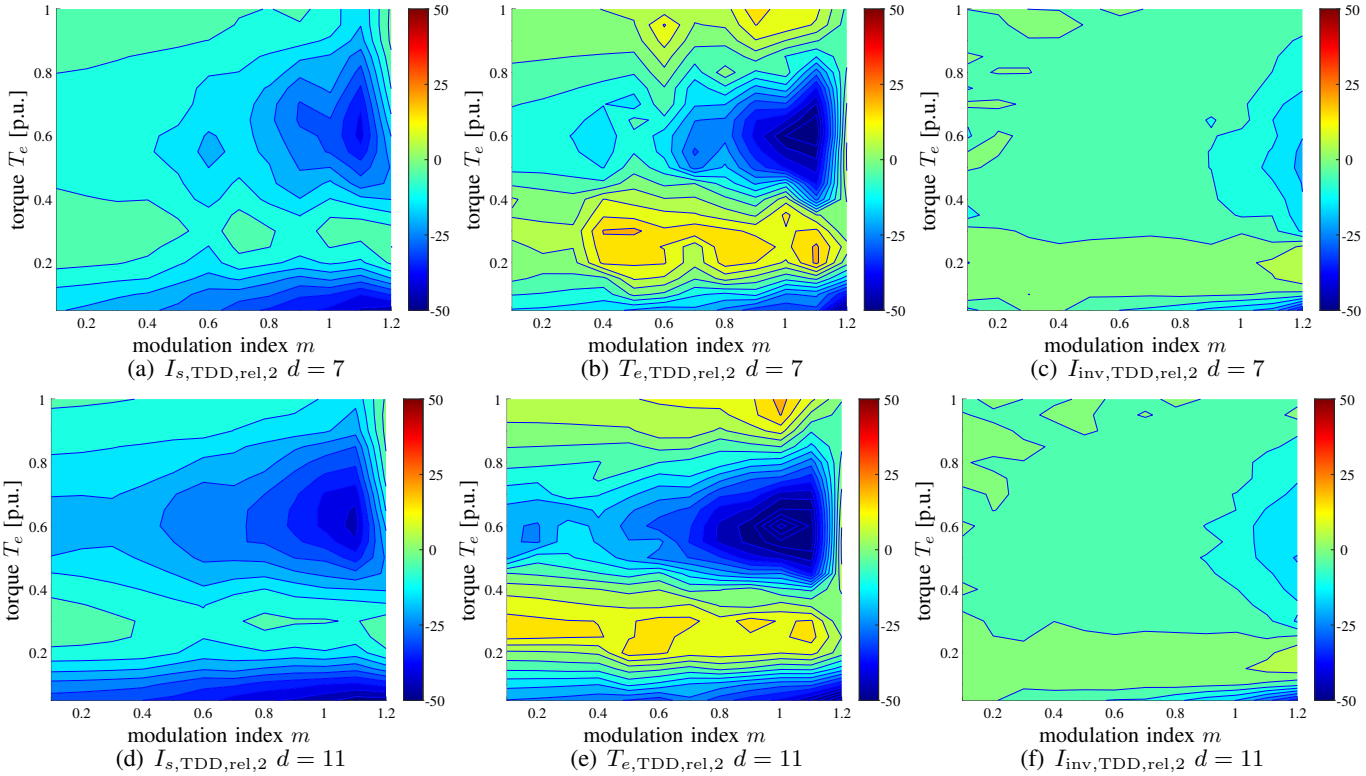

(a) $I_{s,\mathrm{TDD,rel},2}$ $d = 7$ (b) $T_{e,\mathrm{TDD,rel},2}$ $d = 7$ (c) $I_{\mathrm{inv,TDD,rel},2}$ $d = 7$

(d) $I_{s,\mathrm{TDD,rel},2}$ $d = 11$ (e) $T_{e,\mathrm{TDD,rel},2}$ $d = 11$ (f) $I_{\mathrm{inv,TDD,rel},2}$ $d = 11$

Fig. 7: Relative performance metrics of the back-EMF anisotropic QaHWS OPPs with respect to isotropic QaHWS OPPs on a motor with non-sinusoidal back-EMF

to 50% and 67% for $d = 7$ and $d = 11$, respectively.

The back-EMF OPPs have a positive effect also on the dc-link current ripple, as a smaller relative TDD results for most operating points. This improvement is more evident in the low-torque/high-speed region; as shown in Section IV, this operating region is the one that is most negatively affected by the back-EMF harmonics, thus the performance benefits of the proposed OPPs become more pronounced there.

Overall, the simulation results reveal the important advantage of considering the distortions of the flux linkage harmonics in the optimization problem. The calculated back-EMF OPPs are pulse patterns that can greatly reduce the harmonic content in the stator current and mitigate the adverse effects of a non-sinusoidal back-EMF. Moreover, in contrast to asynchronous modulation solutions, OPPs are applicable over the whole range of modulation indices, thus they can fully utilize the available voltage. Hence, the favorable performance achieved by OPPs can be achieved for the whole operating regime.

VI. Conclusion

Spatial harmonics resulting from construction imperfections can aggravate the adverse effects of switching harmonics. As a result, they can deteriorate the performance of the drive and introduce thermal losses in the motor. To address this issue, this paper proposes a synchronous modulation method designed in the framework of OPPs. Specifically, the concept of conventional OPPs is extended by accurately modeling the load. This is done by deriving analytical expressions for the stator phase currents while accounting for the magnetic anisotropy and the rotor flux linkage harmonics. In doing so, the proposed OPPs can effectively deal with the non-idealities of the load, and thus result in superior current quality, especially at high speeds where the effect of back-EMF harmonic becomes more pronounced. Consequently, the thermal losses in the motor can be reduced, extending the lifetime of the electric drive system. This favorable performance of the proposed OPPs is particularly important as asynchronous modulation methods that can mitigate the negative effect of a non-sinusoidal back-EMF are not effective at low pulse numbers.

References

[1] P. Kshirsagar and R. Krishnan, "High-efficiency current excitation strategy for variable-speed nonsinusoidal back-EMF PMSM machines," *IEEE Trans. Ind. Appl.*, vol. 48, no. 6, pp. 1875–1889, Nov./Dec. 2012.

[2] C. Xia, Y. Xiao, W. Chen, and T. Shi, "Torque ripple reduction in brushless dc drives based on reference current optimization using integral variable structure control," *IEEE Trans. Ind. Electron.*, vol. 61, no. 2, pp. 738–752, Feb. 2014.

[3] H. Kim, Y. Han, K. Lee, and S. Bhattacharya, "A sinusoidal current control strategy based on harmonic voltage injection for harmonic loss reduction of PMSMs with non-sinusoidal back-EMF," *IEEE Trans. Ind. Appl.*, vol. 56, no. 6, pp. 7032–7043, Nov./Dec. 2020.

[4] L. Wang, Z. Q. Zhu, H. Bin, and L. M. Gong, "Current harmonics suppression strategy for PMSM with nonsinusoidal back-EMF based on adaptive linear neuron method," *IEEE Trans. Ind. Electron.*, vol. 67, no. 11, pp. 9164–9173, Nov. 2020.

[5] G. S. Buja and G. B. Indri, "Optimal pulsewidth modulation for feeding ac motors," *IEEE Trans. Ind. Appl.*, vol. IA-13, no. 1, pp. 38–44, Jan./Feb. 1977.

[6] G. S. Buja, "Optimum output waveforms in PWM inverters," *IEEE Trans. Ind. Appl.*, vol. IA-16, no. 6, pp. 830–836, Nov./Dec. 1980.

[7] E. Kontodinas, A. Kraemer, H.-D. Endres, S. Wendel, P. Karamanakos, and J. Bonifacio, "An experimental assessment of modulation methods for drive trains used in electric vehicles," in *Proc. IEEE Ind. Electron. Conf.*, Brussels, Belgium, Oct. 2022, pp. 1–6.

[8] A. Birda, J. Reuss, and C. M. Hackl, "Synchronous optimal pulsewidth modulation for synchronous machines with highly operating point dependent magnetic anisotropy," *IEEE Trans. Ind. Electron.*, vol. 68, no. 5, pp. 3760–3769, May 2021.

[9] Z. Zhang, X. Ge, Z. Tian, X. Zhang, Q. Tang, and X. Feng, "A PWM for minimum current harmonic distortion in metro traction PMSM with saliency ratio and load angle constrains," *IEEE Trans. Power Electron.*, vol. 33, no. 5, pp. 4498–4511, May 2018.

[10] A. Krämer, "Verfahren zum Optimieren eines Pulsmusters zum Ansteuern eines Wechselrichters," Mar. 2023, DE 102023202008.4.

[11] E. Kontodinas, P. Karamanakos, A. Kraemer, and S. Wendel, "Optimized pulse patterns for anisotropic synchronous machines," in *Proc. IEEE Int. Conf. Compatib., Power Electron. and Power Eng.*, Tallinn, Estonia, Jun. 2023, pp. 1–6.